Bioconjugate Chemistry

pubs.acs.org/bc

Article

Complex DNA Architectonics—Self-Assembly of Amphiphilic Oligonucleotides into Ribbons, Vesicles, and Asterosomes

Simon Rothenbühler, Ioan Iacovache, Simon M. Langenegger, Benoît Zuber, and Robert Häner*

Cite This: *Bioconjugate Chem.* 2023, 34, 70−77

Read Online

ACCESS | Metrics & More | Article Recommendations | Supporting Information

ABSTRACT: The precise arrangement of structural subunits is a key factor for the proper shape and function of natural and artificial supramolecular assemblies. In DNA nanotechnology, the geometrically well-defined double-stranded DNA scaffold serves as an element of spatial control for the precise arrangement of functional groups. Here, we describe the supramolecular assembly of chemically modified DNA hybrids into diverse types of architectures. An amphiphilic DNA duplex serves as the sole structural building element of the nanosized supramolecular structures. The morphology of the assemblies is governed by a single subunit of the building block. The chemical nature of this subunit, i.e., polyethylene glycols of different chain length or a carbohydrate moiety, exerts a dramatic influence on the architecture of the assemblies. Cryo-electron microscopy revealed the arrangement of the individual DNA duplexes within the different constructs. Thus, the morphology changes from vesicles to ribbons with increasing length of a linear polyethylene glycol. Astoundingly, attachment of a *N*-acetylgalactosamine carbohydrate to the DNA duplex moiety produces an unprecedented type of star-shaped architecture. The novel DNA architectures presented herein imply an extension of the current concept of DNA materials and shed new light on the fast-growing field of DNA nanotechnology.

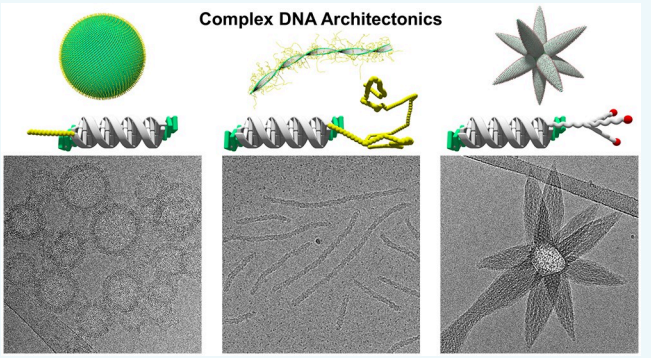

INTRODUCTION

Biochemical processes generally rely on the precise arrangement of the molecular subunits within a hierarchically ordered supramolecular assembly held together by noncovalent, directional interactions.[1] Illustrative examples are natural light-harvesting complexes, in which the spatial organization of the chromophores is crucial for an efficient transfer of excitation energy within large protein complexes.[2,3] In nanotechnology, DNA is widely used as a structural element for the bottom-up assembly of nanostructures because the scaffold of the DNA duplex serves as a versatile, robust, and yet highly reliable tool of spatial control.[4−6] The specificity and programmability of nucleic acid folding enables the bottom-up creation of multidimensional structures by the DNA origami approach.[7−14] Alternatively, DNA nanostructures can be constructed by a self-assembly approach using DNA tiles with sticky ends.[15−19] Despite their elegance, both approaches face some limitations, because they often require a set of many, even up to hundreds, different DNA sequences to assemble a desired nanostructure.[20] The integration of unnatural nucleotide surrogates into oligonucleotides introduces additional functionality and extends the scope of application of DNA from the biological context to the field of materials sciences.[21−30] Chemically modified DNA conjugates were shown to form supramolecular polymers with potential applications, e.g., in biomedicine for drug delivery systems or in optoelectronic devices.[31−40] Recently, we reported the supramolecular assembly of amphiphilic DNA, bearing either phenanthrene or tetraphenylethylene (TPE) hydrophobic ends, into vesicle-shaped objects.[41,42] Hydrophobic interactions of DNA sticky ends, as well as spermine-mediated electrostatic interactions,[43,44] are among the driving forces that lead to the formation of these DNA-constructed vesicles. Besides serving as sticky ends, hydrophobic TPE overhangs also permit the direct observation of the self-assembly process by fluorescence spectroscopy due to their aggregation-induced emission (AIE) properties.[45−47] Potential applications of vesicles consisting of a DNA-constructed membrane comprise, among others, the use as delivery vehicles for biologically active compounds. We therefore explored the effects of modification of the amphiphilic TPE-derived DNA duplex with additional terminal bioconjugate groups that are, e.g., applied in liposome-based drug delivery systems. Here, we describe the profound effects of such bioconjugates, poly-

Special Issue: Chemistry of DNA Nanotechnology

Received: February 11, 2022
Revised: March 15, 2022
Published: March 31, 2022

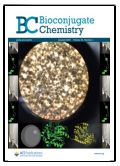

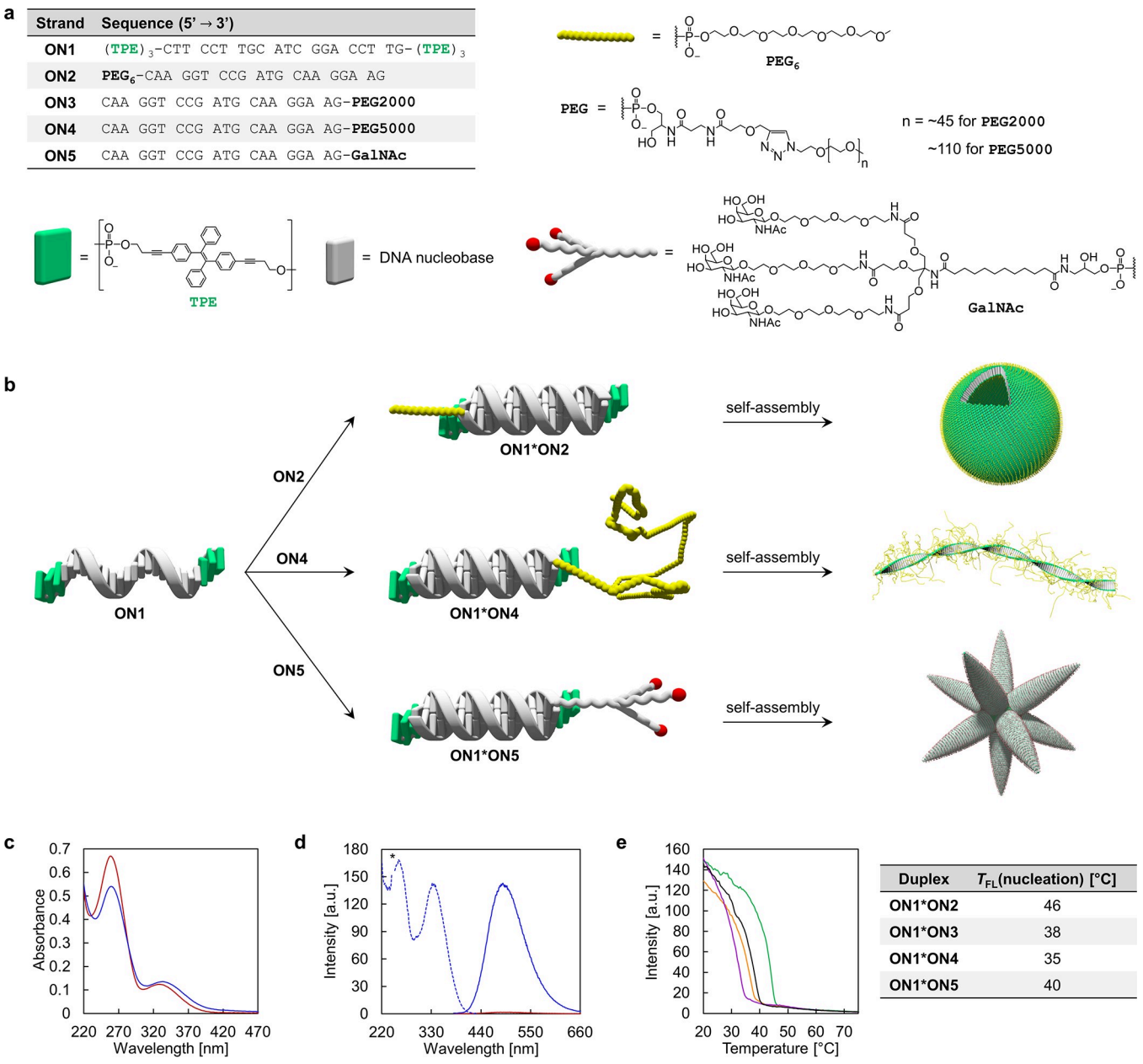

Duplex	T_{FL}(nucleation) [°C]
ON1*ON2	46
ON1*ON3	38
ON1*ON4	35
ON1*ON5	40

Figure 1. Architectonics of DNA conjugates. (a) Sequences of oligomers and chemical structures of modifications. (b) TPE modified single strand **ON1** leads to the formation of diverse DNA architectures after hybridization with different complements. (c,d) Temperature-dependent UV−vis absorption (c), fluorescence emission (d, solid line), and excitation (d, dotted line) spectra of **ON1*ON5** at 75 °C (red) and at 20 °C (blue) after thermally controlled assembly (0.5 °C/min; * denotes second-order diffraction). (e) Fluorescence-monitored annealing curves of **ON1*ON2** (green), **ON1*ON3** (orange), **ON1*ON4** (purple), and **ON1*ON5** (black) including their respective nucleation temperatures T_{FL}(nucleation) [Nucleation temperature determined by sharp fluorescence onset in cooling curves.] Conditions for (c−e): 1 μM each single strand, 10 mM sodium phosphate buffer pH 7.2, 0.1 mM spermine·4 HCl, 30 vol % ethanol, λ_{ex}: 335 nm, λ_{em}: 490 nm, gradient: 0.5 °C/min.

ethylene glycol (PEG) chains of different length and a carbohydrate-based moiety, on the DNA-based architectures.

RESULTS AND DISCUSSION

Supramolecular Assembly of Amphiphilic DNA into Different Types of Architectures. The DNA conjugates studied in this work are displayed in Figure 1a. The TPE-modified oligonucleotide **ON1** was prepared via solid-phase synthesis and purified by HPLC following published procedures (see Supporting Information).[42] The oligonucleotide contains three phosphodiester-linked TPE moieties at the 3′- and 5′-ends. Oligonucleotides **ON2** and **ON5** were purchased from commercial suppliers. PEG-DNA conjugates **ON3** and **ON4** were prepared via copper-catalyzed azide−alkyne cycloaddition from the commercially available 3′-modified alkyne oligonucleotide and the corresponding methoxy-PEG (mPEG) azides.[48] mPEG2000 azide (PEG average M_n 2000 Da) and mPEG5000 azide (PEG average M_n 5000 Da) were used for the preparation of **ON3** and **ON4**, respectively, to yield the PEG-DNA conjugates.

Hybridization of **ON1** with any of the complementary oligonucleotides **ON2**−**ON5** leads to DNA duplexes with TPE overhangs (sticky ends) at both ends (Figure 1b). A further

https://doi.org/10.1021/acs.bioconjchem.2c00077
Bioconjugate Chem. 2023, 34, 70−77

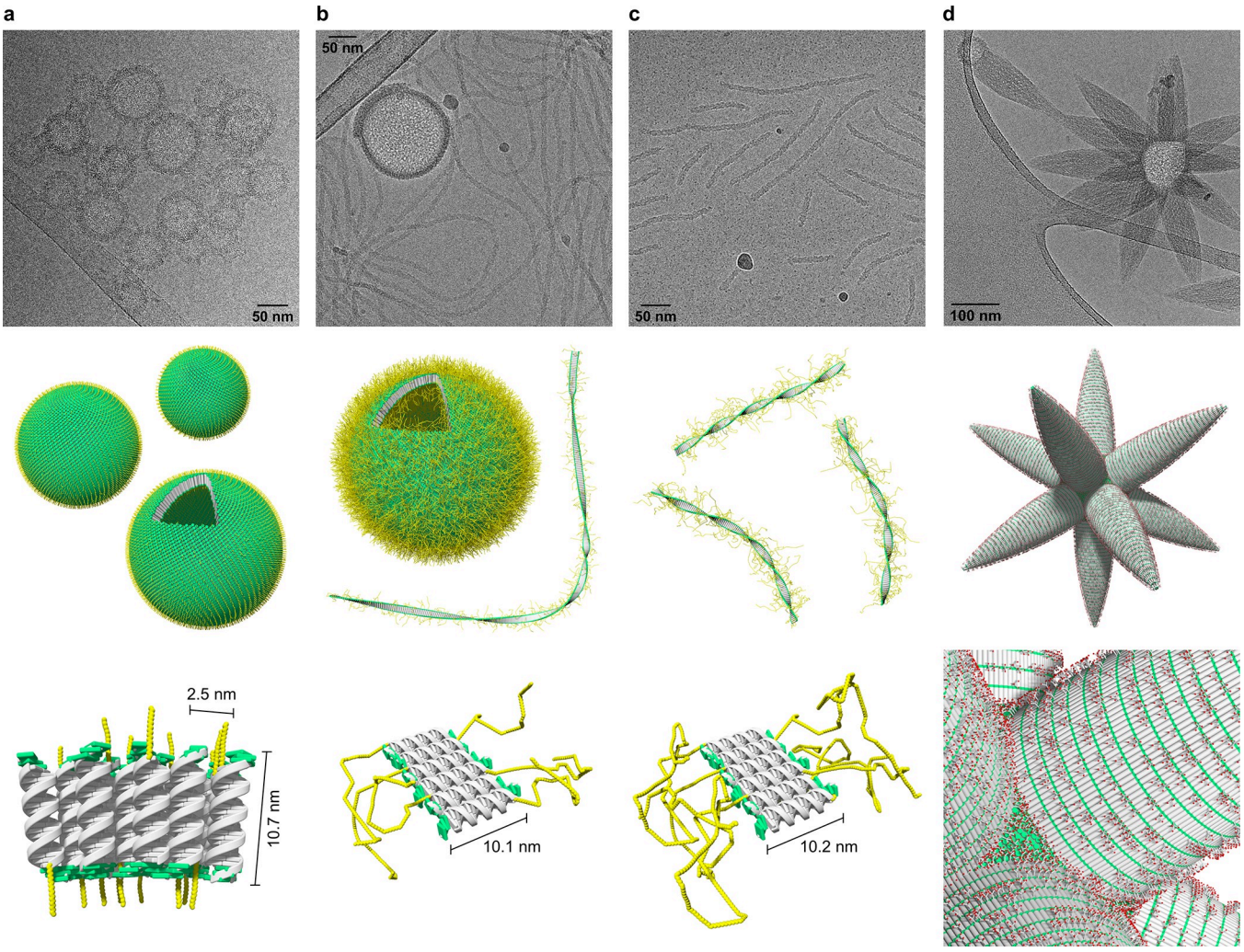

Figure 2. Impact of terminal functionalities on the supramolecular DNA architecture revealed by cryo-EM imaging. (a) Formation of unilamellar vesicles by self-assembly of **ON1*ON2**. (b) Coexistence of ribbons and vesicles after self-assembly of **ON1*ON3**. (c) Duplex **ON1*ON4** assembles into ribbons only. (d) Self-assembly of **ON1*ON5** leads to the formation of star-like nanoobjects (asterosomes). Conditions for (a–d): 1 μM each single strand, 10 mM sodium phosphate buffer pH 7.2, 0.1 mM spermine·4 HCl, 30 vol % ethanol; see Supporting Information for additional images.

functionality, a PEG or carbohydrate moiety, is attached to the DNA complement, as illustrated in Figure 1b.

Supramolecular assembly of duplex **ON1*ON5** is monitored by temperature-dependent UV–vis spectra (Figure 1c) showing a hypochromic effect around 260 nm (DNA and TPE absorption), together with a bathochromic shift of the absorption band from 328 to 333 nm (TPE absorption only) upon cooling (0.5 °C/min). Temperature-dependent fluorescence emission spectra of **ON1*ON5** further support the formation of supramolecular assemblies at 20 °C (Figure 1d). At 75 °C, only a marginal emission is detected upon TPE excitation (λ_{ex}: 335 nm) and in agreement with AIE; this implies that duplex **ON1*ON5** is entirely disassembled into separate DNA single strands **ON1** and **ON5**. After cooling to 20 °C, TPE aggregation results in a strong fluorescence signal (centered around 490 nm). The start of the supramolecular assembly process upon cooling of the solution is indicated by a sharp increase in fluorescence. The nucleation temperatures [T_{FL}(nucleation)] of the four different duplexes range between 35 and 46 °C as shown in the corresponding fluorescence-monitored annealing curves (Figure 1e).

Effects of DNA-PEGylation on Supramolecular Architecture. PEGylation of oligonucleotides is a frequently used method for the improvement of the pharmacokinetic properties of therapeutic oligonucleotides.[49] The stealth properties of PEG protect oligonucleotides from undesired interactions with enzymes and, thus, from nucleolytic degradation.[50]

As demonstrated by cryo-electron microscopy (cryo-EM), duplex **ON1*ON2**, which is functionalized with a short terminal PEG_6 chain, self-assembles into vesicular constructs after thermal assembly (Figure 2a). The size of the vesicles ranges between 50 and 100 nm in diameter. The thickness of the vesicular membrane was determined to be 10.7 ± 0.6 nm, which correlates with the length of a 26-mer DNA duplex and is well in agreement with a previously reported, comparable architecture.[42] The membrane thickness evidences the presence of unilamellar vesicles formed by a compact, columnar arrangement of **ON1*ON2** duplexes. The columnar packing of the DNA is further supported by a regular pattern which is arranged perpendicular to the vesicular membrane. A distance of 2.5 ± 0.3 nm was measured between the parallel aligned rods, which matches the width of a single DNA duplex

https://doi.org/10.1021/acs.bioconjchem.2c00077
Bioconjugate Chem. 2023, 34, 70–77

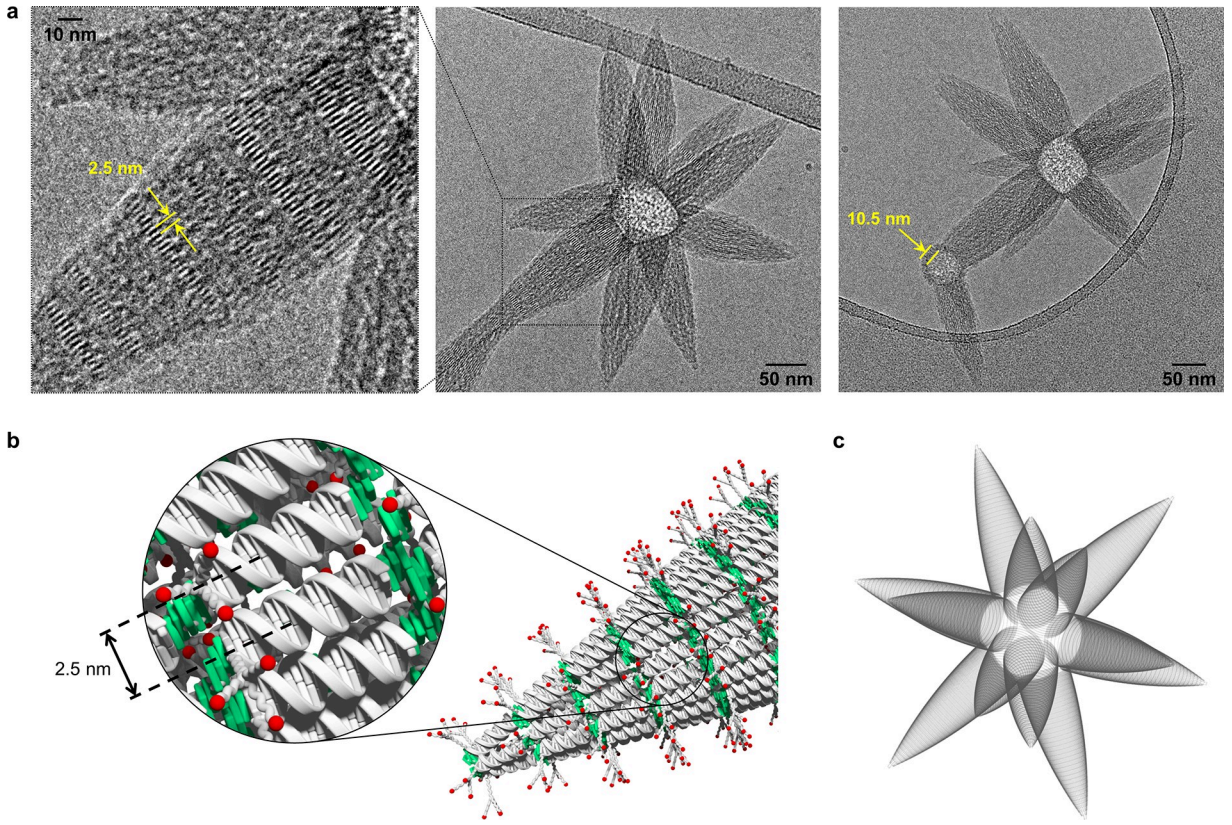

Figure 3. Asterosomes formed via supramolecular assembly of triantennary GalNAc-functionalized DNA conjugate **ON1*ON5**. (a) Cryo-EM images of self-assembled **ON1*ON5**. Conditions: 1 μM **ON1*ON5**, 10 mM sodium phosphate buffer pH 7.2, 0.1 mM spermine·4 HCl, 30 vol % ethanol. (b) Illustration of the extended DNA duplex alignment in the cones. (c) Shadow image created from a dodecahedral arrangement of cones.

(Figure 2a, illustration). We assume that the PEG_6 chains randomly point toward the inside and outside of the vesicles, thus covering both sides with a thin PEG layer. Cryo-EM imaging shows considerable agglomeration of individual vesicles. Likely, the PEG_6 chain is too short to shield individual vesicles entirely from hydrophobic surface interactions.

Duplex **ON1*ON3**, which contains a PEG2000 chain, substantially changes the predominant morphology of the nanostructures (Figure 2b). While cryo-EM imaging still shows the rare occurrence of vesicles, the main type of supramolecular structure now appears as ribbons. The vesicles of **ON1*ON3** exhibit the same kind of DNA packing as those assembled from **ON1*ON2** (Figure 2a) and the distance measurements are nearly identical with a membrane thickness of 10.0 ± 0.5 nm and a DNA width of 2.4 ± 0.3 nm. The only observable difference resides in a somewhat larger diameter of 100 to 200 nm, which is about twice the diameter observed for vesicles of **ON1*ON3**. The ribbons exhibit an overall thickness of 10.1 ± 0.7 nm, which again corresponds very well to the length of the DNA duplex. Therefore, a side-by-side duplex alignment as depicted schematically in (Figure 2b) can be reasonably assigned. The ribbons extend over very long distances, in some cases over a few micrometers.

The coexistence of vesicles and ribbons observed after increasing the size of the PEG chains directed us to test the effect of even longer PEG chains (PEG5000, 110 units). As anticipated, this duplex leads to the formation of ribbons only (Figure 2c). Again, the ribbons possess a thickness of 10.2 ± 0.7 nm, which is similar to the ribbons assembled from **ON1*ON3** and, thus, suggests an identical duplex alignment as illustrated in Figure 2c. However, ribbons of **ON1*ON4** are considerably shorter than the ones formed by **ON1*ON3** (usually less than 350 nm). The long PEG5000 chains are assumed to wrap around individual DNA duplexes and the integration of these wrapped duplexes into the supramolecular ribbons is impeded. This assumption is supported experimentally by the presence of small dark spots (encircled in Figure S21) present in the cryo-EM images, which might be ascribed to individual DNA duplexes.

Conjugation of a Branched Carbohydrate Moiety Leads to Fundamental Morphological Changes. We next turned our attention to the modification of the DNA duplex with a branched tricarbohydrate moiety. In addition to presumably enhance the potential bioapplications of the supramolecular assemblies, the *N*-acetylgalactosamine (GalNAc) moiety is, due to its branched nature, also sterically more demanding than the linear PEG chains (Figure 1). The aspect of surface crowding is believed to have a strong impact on the supramolecular assembly, as described below.[51] The trivalent GalNAc DNA conjugate **ON5** was selected due to its well-documented potential for targeted delivery of GalNAc conjugated nucleic acids, in particular, short interfering RNAs (siRNAs), to hepatocytes.[52−54] This ligand exhibits an excellent binding affinity toward the asialoglycoprotein receptor (ASGR), which is abundantly expressed in hepatocytes and, thus, responsible for the targeted delivery.[55]

Much to our surprise, the supramolecular assembly of **ON1*ON5** leads to an entirely different and novel type of DNA architecture. Cryo-EM imaging (Figure 2d) discloses star-like, or mace-like, supramolecular polymers, in which

https://doi.org/10.1021/acs.bioconjchem.2c00077
Bioconjugate Chem. 2023, 34, 70−77

multiple parabolic cone-shaped extensions are pointing outward from the center of the object. Due to their star-shaped appearance, we will refer to these objects as *asterosomes*. The number of cones varies among individual asterosomes. The center of the structures appears spherical, and for small spheres, only one or two cones are present. In larger objects, roughly up to 12 protrusions are observed, in which case their arrangement can be approximated by a small stellated dodecahedron.[56] Noteworthy, a vesicular membrane is visible around the base of the parabolic cone(s) of structures with only a small number of extensions. The thickness of this membrane amounts to 10.5 ± 0.5 nm, which is consistent with a unilamellar, columnar DNA duplex alignment. The width of the cones at their base ranges between 50 and 75 nm. Regular patterns of discrete bands, which are clearly visible in some areas (Figure 3a), reveal the arrangement of the DNA in the cones. These bands are formed by parallel aligned rods with a distance between these rods of 2.5 ± 0.2 nm (illustration Figure 3b), which corresponds again to the width of the DNA duplex. Hence, the discrete bands are formed by parallel aligned DNA duplexes which, in turn, leads to the conclusion that the cones are characterized by an extended duplex alignment, as illustrated in Figure 3b. Interaction between the DNA segments is ensured by the hydrophobic sticky ends. In the images, the cones of individual asterosomes appear to be of different lengths. Cryo-EM imaging is a projection of three-dimensional (3D) objects onto a two-dimensional (2D) plane, which may lead to a perceived asymmetry of rather uniform-sized cones. To test this possibility, we used a shadow image to simulate the appearance of a regular asterosome at an arbitrary perspective. Regular is defined here as derived from the platonic body (dodecahedron) with all cones pointing toward the center of the surface planes (pentagon). The resulting shadow image of the modeled dodecahedron-type asterosome is depicted in Figure 3c. The obvious similarity between modeled and found pattern suggests that the cones of an individual asterosome are rather uniform in size.

Taking all the morphological features into consideration, we assume that the star-like morphology evolves in a two-step process. Thus, columnar packed vesicular constructs of varying sizes are formed in the first phase of the assembly process. It can be assumed that the trivalent GalNAc moieties lead to a steric crowding on the surface of the vesicles. The resulting strain can be reduced by the formation of the cones. This involves a change of the supramolecular organization from the columnar packing to the extended arrangement of the DNA units. The transition from columnar to extended arrangement results in a significant surface enlargement, hence a redistribution of the bulky GalNAc moieties over a wider area along with a reduction of surface crowding. The growth of the cones can be imagined as a telescopic slide-out process, during which the columnar aligned DNA duplexes slide along each other until reaching the extended arrangement (see SI Video for further illustration). This hypothesis is supported by two additional aspects. First, the number of DNA duplexes assembled in one cone matches roughly the number of duplexes that would be present within the curved surface area of the columnar packed vesicle. Second, fewer cones evolve from small vesicles; the smaller the vesicle, the higher the curvature, and hence, a smaller surface crowding between the branched GalNAc moieties is assumed.

Atomic force microscopy (AFM) was utilized to validate the different morphologies observed by cryo-EM imaging and further support the findings (Figures S24−S26). Vesicles with a size range consistent with the ones detected by cryo-EM were observed for self-assembled **ON1*ON2**. For the ribbons assembled from **ON1*ON3**, the average height is around 1 nm, which is less than expected for the width of a single DNA duplex. However, such a flattening has been described in the literature and is probably due to the AFM tip convolution effect.[57] Finally, AFM imaging also provided independent evidence of star-shaped objects formed by self-assembly of **ON1*ON5** with clearly discernible cones, albeit with lower resolution than cryo-EM.

CONCLUSION

In conclusion, the supramolecular assembly of amphiphilic DNA conjugates into three distinct, well-defined DNA architectures has been demonstrated. Vesicles, ribbons, and star-shaped objects (asterosomes) are assembled from DNA duplexes formed of a tetraphenylethylene-oligonucleotide and single-stranded complements bearing various types of terminal functionalities. The terminal functionalities dictate the supramolecular assembly process and account for the emergence of the diverse morphologies. Cryo-EM imaging revealed precise information on the exact DNA duplex arrangements within the nanostructures. A morphological change from unilamellar vesicles to ribbons was observed when the length of linear PEG was increased. The use of a trivalent GalNAc moiety in combination with the amphiphilic DNA resulted in a fundamental morphological change. The supramolecular self-assembly of this DNA duplex led to the formation of star-shaped nanostructures (asterosomes), which are characterized by cones emerging radially from the center of the nanoobject. The driving force for the formation of this nanostructure is best explained by a reduction of surface crowding effected by a switch of the DNA duplex alignment from a compact to an extended arrangement during the formation of the cones. A model for the evolution of the cones is presented. So far, comparable star-shaped structures were only reported based on either nanoparticles[58,59] or colloidal clusters,[60,61] whereas all types of structures presented here represent DNA-built, self-supported architectures. Ongoing research aims at the exploration of the presented vesicular DNA architectures as nanocarriers for drug delivery applications and the investigation of excitation energy transfer along the ribbons to an acceptor dye, creating artificial light-harvesting systems.

METHODS

Spectroscopic Measurements. Spectroscopic data were collected from 5 min thermally equilibrated samples at the corresponding temperature using quartz cuvettes with an optical path of 1 cm. UV−vis spectra were measured on an Agilent Cary 100 spectrophotometer, equipped with a Peltier-thermostated multicell holder. Fluorescence spectra were recorded on a Cary Eclipse fluorescence spectrophotometer, equipped with a Peltier-thermostated multicell holder, using an excitation slit of 2.5 nm and an emission slit of 5 nm.

Thermally Controlled Assembly Process. Supramolecular assembly of the DNA architectures was accomplished via thermal disassembly and controlled reassembly. Therefore, the sample solution was heated to 75 °C, before cooling the solution to 20 °C with a gradient of 0.5 °C/min in a Cary Eclipse fluorescence spectrophotometer equipped with a Peltier-thermostated multicell holder. Samples for cryo-EM

https://doi.org/10.1021/acs.bioconjchem.2c00077
Bioconjugate Chem. 2023, 34, 70−77

and AFM were prepared directly after the thermal assembly process.

Cryo-EM Image Acquisition and Analysis. Samples for cryo-EM were plunge-frozen using the FEI Vitrobot Mark 4 at room temperature and 100% humidity. In brief, copper lacey carbon grids were glow-discharged (air −10 mA for 20 s). Three microliters of the sample was pipetted on the grids and blotted for 3 s before plunging into liquid ethane. Sample grids were stored in liquid nitrogen. Images were acquired using a Gatan 626 cryo holder on a Falcon III equipped FEI Tecnai F20 in nanoprobe mode. Due to the nature of the sample, acquisition settings had to be adjusted for a low total electron dose (less than 20 $e^-/Å^2$) using EPU software. Distance measurements were done in Fiji[62,63] using the multipoint tool to set marks. After the readout of the *x*- and *y*-values, the distances between the marks were calculated. The reported distances are mean values with the corresponding standard deviation. A summary of all measured distances as well as representative graphical descriptions where the measurements have been done is provided in the Supporting Information.

Shadow Image. The shadow image was rendered in POV-Ray 3.7 (official POV-Ray Web site: www.povray.org). In brief, the image was created from a dodecahedral 3D assembly, constructed from light-absorbing medium; the triantennary GalNAc linkers were neglected for simplification. Afterward, the 3D illustration was rotated into an arbitrary orientation. The 3D assembly was irradiated with parallel light, orthogonal to the shadow plane, which afforded the shadow image.

AFM Imaging. AFM experiments were conducted on a Nanosurf FlexAFM instrument in tapping mode under ambient conditions. Tap190Al-G cantilevers from Budget-Sensors, Innovative Solutions Bulgaria Ltd. were used. AFM samples were prepared on APTES-modified mica sheets (Glimmer "V1", 20 mm × 20 mm, G250-7, Plano GmbH) according to published procedures, using a sample adsorption time of 7 min.[42,64] APTES, (3-aminopropyl)triethoxysilane.

■ ASSOCIATED CONTENT

Supporting Information

The Supporting Information is available free of charge at https://pubs.acs.org/doi/10.1021/acs.bioconjchem.2c00077.

DNA conjugates synthesis, UV−vis and fluorescence spectra, additional cryo-EM, and AFM images (PDF)

Animation of *asterosome*-cone growth (MP4)

■ AUTHOR INFORMATION

Corresponding Author

Robert Häner − *Department of Chemistry, Biochemistry and Pharmaceutical Sciences, University of Bern, CH-3012 Bern, Switzerland;* orcid.org/0000-0001-5014-4318; Email: robert.haener@unibe.ch

Authors

Simon Rothenbühler − *Department of Chemistry, Biochemistry and Pharmaceutical Sciences, University of Bern, CH-3012 Bern, Switzerland;* orcid.org/0000-0002-6212-2295

Ioan Iacovache − *Institute of Anatomy, University of Bern, CH-3012 Bern, Switzerland*

Simon M. Langenegger − *Department of Chemistry, Biochemistry and Pharmaceutical Sciences, University of Bern, CH-3012 Bern, Switzerland*

Benoît Zuber − *Institute of Anatomy, University of Bern, CH-3012 Bern, Switzerland;* orcid.org/0000-0001-7725-5579

Complete contact information is available at: https://pubs.acs.org/10.1021/acs.bioconjchem.2c00077

Notes

The authors declare no competing financial interest.

■ ACKNOWLEDGMENTS

Financial support by the Swiss National Foundation (200020_188468 to R.H. and 31003A_179520 to B.Z.) is gratefully acknowledged. Cryo-electron microscopy was performed on equipment supported by the Microscopy Imaging Center (MIC), University of Bern, Switzerland.

■ REFERENCES

(1) van der Zwaag, D.; Meijer, E. W. Fueling Connections between Chemistry and Biology. *Science* **2015**, *349* (6252), 1056−1057.

(2) Lambrev, P. H.; Várkonyi, Z.; Krumova, S.; Kovács, L.; Miloslavina, Y.; Holzwarth, A. R.; Garab, G. Importance of Trimer-Trimer Interactions for the Native State of the Plant Light-Harvesting Complex II. *Biochim. Biophys. Acta* **2007**, *1767* (6), 847−853.

(3) Engel, G. S.; Calhoun, T. R.; Read, E. L.; Ahn, T. K.; Mančal, T.; Cheng, Y.-C.; Blankenship, R. E.; Fleming, G. R. Evidence for Wavelike Energy Transfer through Quantum Coherence in Photosynthetic Systems. *Nature* **2007**, *446* (7137), 782−786.

(4) Seeman, N. C. DNA in a Material World. *Nature* **2003**, *421*, 427−431.

(5) Brady, R. A.; Brooks, N. J.; Cicuta, P.; Di Michele, L. Crystallization of Amphiphilic DNA C-Stars. *Nano Lett.* **2017**, *17* (5), 3276−3281.

(6) Fabrini, G.; Minard, A.; Brady, R. A.; Di Antonio, M.; Di Michele, L. Cation-Responsive and Photocleavable Hydrogels from Noncanonical Amphiphilic DNA Nanostructures. *Nano Lett.* **2022**, *22* (2), 602−611.

(7) Rothemund, P. W. K. Folding DNA to Create Nanoscale Shapes and Patterns. *Nature* **2006**, *440*, 297−302.

(8) Kim, D.-N.; Kilchherr, F.; Dietz, H.; Bathe, M. Quantitative Prediction of 3D Solution Shape and Flexibility of Nucleic Acid Nanostructures. *Nucleic Acids Res.* **2012**, *40* (7), 2862−2868.

(9) Dey, S.; Fan, C.; Gothelf, K. V.; Li, J.; Lin, C.; Liu, L.; Liu, N.; Nijenhuis, M. A. D.; Saccà, B.; Simmel, F. C.; et al. DNA Origami. *Nat. Rev. Methods Prim* **2021**, *1*, 13.

(10) Schill, J.; Rosier, B. J. H. M.; Audenis, B. G.; Estirado, E. M.; de Greef, T. F. A.; Brunsveld, L. Assembly of Dynamic Supramolecular Polymers on a DNA Origami Platform. *Angew. Chem. Int. Ed* **2021**, *60* (14), 7612−7616.

(11) Veneziano, R.; Moyer, T. J.; Stone, M. B.; Wamhoff, E.-C.; Read, B. J.; Mukherjee, S.; Shepherd, T. R.; Das, J.; Schief, W. R.; Irvine, D. J.; et al. Role of Nanoscale Antigen Organization on B-Cell Activation Probed Using DNA Origami. *Nat. Nanotechnol* **2020**, *15* (8), 716−723.

(12) Thomsen, R. P.; Malle, M. G.; Okholm, A. H.; Krishnan, S.; Bohr, S. S. R.; Sørensen, R. S.; Ries, O.; Vogel, S.; Simmel, F. C.; Hatzakis, N. S.; et al. A Large Size-Selective DNA Nanopore with Sensing Applications. *Nat. Commun.* **2019**, *10*, 5655.

(13) Wolfrum, M.; Schwarz, R. J.; Schwarz, M.; Kramer, M.; Richert, C. Stabilizing DNA Nanostructures through Reversible Disulfide Crosslinking. *Nanoscale* **2019**, *11* (31), 14921−14928.

(14) Noteborn, W. E. M.; Abendstein, L.; Sharp, T. H. One-Pot Synthesis of Defined-Length SsDNA for Multiscaffold DNA Origami. *Bioconjugate Chem.* **2021**, *32* (1), 94−98.

(15) Chen, J.; Seeman, N. C. Synthesis from DNA of a Molecule with the Connectivity of a Cube. *Nature* **1991**, *350*, 631−633.

(16) Huang, K.; Yang, D.; Tan, Z.; Chen, S.; Xiang, Y.; Mi, Y.; Mao, C.; Wei, B. Self-Assembly of Wireframe DNA Nanostructures from Junction Motifs. *Angew. Chem. Int. Ed* **2019**, *58* (35), 12123−12127.
(17) Taylor, L. L. K.; Riddell, I. A.; Smulders, M. M. J. Self-Assembly of Functional Discrete Three-Dimensional Architectures in Water. *Angew. Chem. Int. Ed* **2019**, *58* (5), 1280−1307.
(18) Yao, G.; Zhang, F.; Wang, F.; Peng, T.; Liu, H.; Poppleton, E.; Šulc, P.; Jiang, S.; Liu, L.; Gong, C.; et al. Meta-DNA Structures. *Nat. Chem.* **2020**, *12* (11), 1067−1075.
(19) Gentile, S.; Del Grosso, E.; Pungchai, P. E.; Franco, E.; Prins, L. J.; Ricci, F. Spontaneous Reorganization of DNA-Based Polymers in Higher Ordered Structures Fueled by RNA. *J. Am. Chem. Soc.* **2021**, *143* (48), 20296−20301.
(20) Seeman, N. C.; Sleiman, H. F. DNA Nanotechnology. *Nat. Rev. Mater.* **2017**, *3*, 17068.
(21) Simeth, N. A.; Kobayashi, S.; Kobauri, P.; Crespi, S.; Szymanski, W.; Nakatani, K.; Dohno, C.; Feringa, B. L. Rational Design of a Photoswitchable DNA Glue Enabling High Regulatory Function and Supramolecular Chirality Transfer. *Chem. Sci.* **2021**, *12* (26), 9207−9220.
(22) Bürki, N.; Grossenbacher, E.; Cannizzo, A.; Feurer, T.; Langenegger, S. M.; Häner, R. DNA-Organized Artificial LHCs - Testing the Limits of Chromophore Segmentation. *Org. Biomol. Chem.* **2020**, *18* (35), 6818−6822.
(23) Goodnow, R. A.; Dumelin, C. E.; Keefe, A. D. DNA-Encoded Chemistry: Enabling the Deeper Sampling of Chemical Space. *Nat. Rev. Drug Discov* **2017**, *16* (2), 131−147.
(24) Burns, J. R.; Göpfrich, K.; Wood, J. W.; Thacker, V. V.; Stulz, E.; Keyser, U. F.; Howorka, S. Lipid-Bilayer-Spanning DNA Nanopores with a Bifunctional Porphyrin Anchor. *Angew. Chem. Int. Ed* **2013**, *52* (46), 12069−12072.
(25) Steinmetzger, C.; Bäuerlein, C.; Höbartner, C. Supramolecular Fluorescence Resonance Energy Transfer in Nucleobase-Modified Fluorogenic RNA Aptamers. *Angew. Chem. Int. Ed* **2020**, *59* (17), 6760−6764.
(26) Madsen, M.; Gothelf, K. V. Chemistries for DNA Nanotechnology. *Chem. Rev.* **2019**, *119* (10), 6384−6458.
(27) Mass, O. A.; Wilson, C. K.; Roy, S. K.; Barclay, M. S.; Patten, L. K.; Terpetschnig, E. A.; Lee, J.; Pensack, R. D.; Yurke, B.; Knowlton, W. B. Exciton Delocalization in Indolenine Squaraine Aggregates Templated by DNA Holliday Junction Scaffolds. *J. Phys. Chem. B* **2020**, *124* (43), 9636−9647.
(28) Gouda, A. S.; Przypis, Ł.; Walczak, K.; Jørgensen, P. T.; Wengel, J. Carbazole Modified Oligonucleotides: Synthesis, Hybridization Studies and Fluorescence Properties. *Org. Biomol. Chem.* **2020**, *18* (35), 6935−6948.
(29) Kropp, H. M.; Diederichs, K.; Marx, A. The Structure of an Archaeal B-Family DNA Polymerase in Complex with a Chemically Modified Nucleotide. *Angew. Chem. Int. Ed* **2019**, *58* (16), 5457−5461.
(30) Zhu, R. Y.; Majumdar, C.; Khuu, C.; De Rosa, M.; Opresko, P. L.; David, S. S.; Kool, E. T. Designer Fluorescent Adenines Enable Real-Time Monitoring of MUTYH Activity. *ACS Cent. Sci.* **2020**, *6* (10), 1735−1742.
(31) Bui, H.; Díaz, S. A.; Fontana, J.; Chiriboga, M.; Veneziano, R.; Medintz, I. L. Utilizing the Organizational Power of DNA Scaffolds for New Nanophotonic Applications. *Adv. Opt. Mater.* **2019**, *7* (18), 1900562.
(32) Mathur, D.; Medintz, I. L. The Growing Development of DNA Nanostructures for Potential Healthcare-Related Applications. *Adv. Healthcare Mater.* **2019**, *8* (9), 1801546.
(33) Keller, A.; Linko, V. Challenges and Perspectives of DNA Nanostructures in Biomedicine. *Angew. Chem. Int. Ed* **2020**, *59* (37), 15818−15833.
(34) Wijnands, S. P. W.; Meijer, E. W.; Merkx, M. DNA-Functionalized Supramolecular Polymers: Dynamic Multicomponent Assemblies with Emergent Properties. *Bioconjugate Chem.* **2019**, *30* (7), 1905−1914.
(35) Ensslen, P.; Gärtner, S.; Glaser, K.; Colsmann, A.; Wagenknecht, H.-A. A DNA-Fullerene Conjugate as a Template for Supramolecular Chromophore Assemblies: Towards DNA-Based Solar Cells. *Angew. Chem. Int. Ed* **2016**, *55* (5), 1904−1908.
(36) Vybornyi, M.; Vyborna, Y.; Häner, R. DNA-Inspired Oligomers: From Oligophosphates to Functional Materials. *Chem. Soc. Rev.* **2019**, *48* (16), 4347−4360.
(37) Zhao, Z.; Du, T.; Liang, F.; Liu, S. Amphiphilic DNA Organic Hybrids: Functional Materials in Nanoscience and Potential Application in Biomedicine. *Int. J. Mol. Sci.* **2018**, *19* (8), 2283.
(38) Märcher, A.; Nijenhuis, M. A. D.; Gothelf, K. V. A Wireframe DNA Cube: Antibody Conjugate for Targeted Delivery of Multiple Copies of Monomethyl Auristatin E. *Angew. Chem. Int. Ed* **2021**, *60* (40), 21691−21696.
(39) Appukutti, N.; Serpell, C. J. High Definition Polyphosphoesters: Between Nucleic Acids and Plastics. *Polym. Chem.* **2018**, *9* (17), 2210−2226.
(40) Zhang, Y.; Peng, R.; Xu, F.; Ke, Y. Hierarchical Self-Assembly of Cholesterol-DNA Nanorods. *Bioconjugate Chem.* **2019**, *30* (7), 1845−1849.
(41) Bösch, C. D.; Jevric, J.; Bürki, N.; Probst, M.; Langenegger, S. M.; Häner, R. Supramolecular Assembly of DNA-Phenanthrene Conjugates into Vesicles with Light-Harvesting Properties. *Bioconjugate Chem.* **2018**, *29* (5), 1505−1509.
(42) Rothenbühler, S.; Iacovache, I.; Langenegger, S. M.; Zuber, B.; Häner, R. Supramolecular Assembly of DNA-Constructed Vesicles. *Nanoscale* **2020**, *12* (41), 21118−21123.
(43) Egli, M. DNA-Cation Interactions: Quo Vadis? *Chem. Biol.* **2002**, *9* (3), 277−286.
(44) Li, J.; Wijeratne, S. S.; Qiu, X.; Kiang, C.-H. DNA under Force: Mechanics, Electrostatics, and Hydration. *Nanomaterials* **2015**, *5* (1), 246−267.
(45) Luo, J.; Xie, Z.; Lam, J. W. Y.; Cheng, L.; Chen, H.; Qiu, C.; Kwok, H. S.; Zhan, X.; Liu, Y.; Zhu, D.; et al. Aggregation-Induced Emission of 1-Methyl-1,2,3,4,5-Pentaphenylsilole. *Chem. Commun.* **2001**, 1740−1741.
(46) Li, S.; Langenegger, S. M.; Häner, R. Control of Aggregation-Induced Emission by DNA Hybridization. *Chem. Commun.* **2013**, *49* (52), 5835−5837.
(47) Liu, H.; Xiong, L. H.; Kwok, R. T. K.; He, X.; Lam, J. W. Y.; Tang, B. Z. AIE Bioconjugates for Biomedical Applications. *Adv. Opt. Mater.* **2020**, *8* (14), 2000162.
(48) Presolski, S. I.; Hong, V. P.; Finn, M. G. Copper-Catalyzed Azide-Alkyne Click Chemistry for Bioconjugation. *Curr. Protoc. Chem. Biol.* **2011**, *3*, 153−162.
(49) Wang, Y.; Wang, D.; Jia, F.; Miller, A.; Tan, X.; Chen, P.; Zhang, L.; Lu, H.; Fang, Y.; Kang, X.; et al. Self-Assembled DNA−PEG Bottlebrushes Enhance Antisense Activity and Pharmacokinetics of Oligonucleotides. *ACS Appl. Mater. Interfaces* **2020**, *12* (41), 45830−45837.
(50) Nerantzaki, M.; Loth, C.; Lutz, J.-F. Chemical Conjugation of Nucleic Acid Aptamers and Synthetic Polymers. *Polym. Chem.* **2021**, *12* (24), 3498−3509.
(51) Stachowiak, J. C.; Hayden, C. C.; Sasaki, D. Y. Steric Confinement of Proteins on Lipid Membranes Can. Drive Curvature and Tubulation. *Proc. Natl. Acad. Sci. U. S. A* **2010**, *107* (17), 7781−7786.
(52) Kulkarni, J. A.; Witzigmann, D.; Thomson, S. B.; Chen, S.; Leavitt, B. R.; Cullis, P. R.; Van der Meel, R. The Current Landscape of Nucleic Acid Therapeutics. *Nat. Nanotechnol* **2021**, *16*, 630−643.
(53) Benizri, S.; Gissot, A.; Martin, A.; Vialet, B.; Grinstaff, M. W.; Barthélémy, P. Bioconjugated Oligonucleotides: Recent Developments and Therapeutic Applications. *Bioconjugate Chem.* **2019**, *30* (2), 366−383.
(54) Springer, A. D.; Dowdy, S. F. GalNAc-SiRNA Conjugates: Leading the Way for Delivery of RNAi Therapeutics. *Nucleic Acid Ther* **2018**, *28* (3), 109−118.
(55) Schmidt, K.; Prakash, T. P.; Donner, A. J.; Kinberger, G. A.; Gaus, H. J.; Low, A.; Østergaard, M. E.; Bell, M.; Swayze, E. E.; Seth,

P. P. Characterizing the Effect of GalNAc and Phosphorothioate Backbone on Binding of Antisense Oligonucleotides to the Asialoglycoprotein Receptor. *Nucleic Acids Res.* **2017**, *45* (5), 2294−2306.
(56) Cayley, A. On Poinsot's Four New Regular Solids. *Philos. Mag* **1859**, *17* (112), 123−128.
(57) Bustamante, C.; Vesenka, J.; Tang, C. L.; Rees, W.; Guthold, M.; Keller, R. Circular DNA Molecules Imaged in Air by Scanning Force Microscopy. *Biochemistry* **1992**, *31* (1), 22−26.
(58) Zhou, J.; Creyer, M. N.; Chen, A.; Yim, W.; Lafleur, R. P. M.; He, T.; Lin, Z.; Xu, M.; Abbasi, P.; Wu, J.; et al. Stereoselective Growth of Small Molecule Patches on Nanoparticles. *J. Am. Chem. Soc.* **2021**, *143* (31), 12138−12144.
(59) Lermusiaux, L.; Many, V.; Barois, P.; Ponsinet, V.; Ravaine, S.; Duguet, E.; Tréguer-Delapierre, M.; Baron, A. Toward Huygens' Sources with Dodecahedral Plasmonic Clusters. *Nano Lett.* **2021**, *21* (5), 2046−2052.
(60) Kim, Y.-J.; Kim, J.-H.; Jo, I.-S.; Pine, D. J.; Sacanna, S.; Yi, G.-R. Patchy Colloidal Clusters with Broken Symmetry. *J. Am. Chem. Soc.* **2021**, *143* (33), 13175−13183.
(61) Liu, X.; Moradi, M.-A.; Bus, T.; Debije, M. G.; Bon, S. A. F.; Heuts, J. P. A.; Schenning, A. P. H. J. Flower-like Colloidal Particles through Precipitation Polymerization of Redox-Responsive Liquid Crystals. *Angew. Chem. Int. Ed* **2021**, *60* (52), 27026−27030.
(62) Schindelin, J.; Arganda-Carreras, I.; Frise, E.; Kaynig, V.; Longair, M.; Pietzsch, T.; Preibisch, S.; Rueden, C.; Saalfeld, S.; Schmid, B.; et al. Fiji: An Open-Source Platform for Biological-Image Analysis. *Nat. Methods* **2012**, *9* (7), 676−682.
(63) Linkert, M.; Rueden, C. T.; Allan, C.; Burel, J.-M.; Moore, W.; Patterson, A.; Loranger, B.; Moore, J.; Neves, C.; MacDonald, D.; et al. Metadata Matters: Access to Image Data in the Real World. *J. Cell Biol.* **2010**, *189* (5), 777−782.
(64) Bösch, C. D.; Langenegger, S. M.; Häner, R. Light-Harvesting Nanotubes Formed by Supramolecular Assembly of Aromatic Oligophosphates. *Angew. Chem. Int. Ed* **2016**, *55* (34), 9961−9964.

https://doi.org/10.1021/acs.bioconjchem.2c00077
Bioconjugate Chem. 2023, 34, 70−77